Preparation of RhOx/$Ce_yPr_{1-y}O_2$ N_2O decomposition catalysts by rhodium nitrate impregnation with different solvents.

V. Rico-Pérez, C. Salinas-Martínez de Lecea, A. Bueno-López*.

Inorganic Chemistry Department. University of Alicante. Ap. 99 E03080. Alicante (Spain)

Abstract

The effect of the solvent (water, ethanol or acetone) used to impregnate $Ce_yPr_{1-y}O_2$ (y = 1, 0.9 or 0.5) supports with rhodium nitrate, in order to prepare N_2O decomposition catalysts, has been studied. RhOx/$Ce_yPr_{1-y}O_2$ catalysts were prepared and characterized by N_2 adsorption at -196 ºC, XRD, Raman spectroscopy, TEM, XPS and H_2-TPR. The activity for N_2O decomposition of the catalysts studied was related with the RhOx-support interaction, and both the nature of the ceria support and of the solvent used for rhodium impregnation affected such interaction. Ceria doping with 10 % praseodymium had a positive effect in the RhOx-support interaction, but the benefit on the catalytic activity was only obtained for water impregnation because the temperature peaks created during calcination of ethanol and acetone-impregnated catalysts promoted $Ce_{0.9}Pr_{0.1}O_2$ and RhOx sintering. The interaction between RhOx and $Ce_{0.5}Pr_{0.5}O_2$ was not as good as that with $Ce_{0.9}Pr_{0.1}O_2$. The best catalyst was obtained by impregnating $Ce_{0.9}Pr_{0.1}O_2$ with a water solution of rhodium. However, if acetone or ethanol must be used for any reason the pure ceria support is more suitable (under the calcination conditions of this study; 250 to 500 ºC at 10 ºC/min) because do not sinters during solvents combustion.

Key words: *Ceria catalyst; Rhodium catalyst; N_2O decomposition; metal-support interaction*

* Corresponding author:
email: agus@ua.es
Tel. +34 600948665
Fax. +34 965903454

1. Introduction.

Ceria-based materials are of interest in catalysis because of their oxygen storage capacity (OSC) and lattice oxygen mobility [1-3]. These properties are dependent of the crystal size and defects, and can be modified by ceria doping. Ceria-based oxides also affect the catalytic behavior of supported metals [4]. In this sense, RhOx supported on praseodymium-doped ceria has showed enhanced N_2O decomposition activity with regard to RhOx catalyst with pure ceria support [5]. Praseodymium doping modifies the properties of the ceria lattice oxygen, lowers metal-oxygen binding energy in the Rh-mixed oxide interface and increases the number of defects (oxygen vacancies) [6].

In previous studies [7, 8], the calcination conditions were modified in order to improve the distribution of rhodium and to enlarge the rhodium-ceria interface of RhO_x/CeO_2 catalysts. Improved catalytic activity for N_2O decomposition and CO oxidation was obtained by flash calcination, which consisted of introducing the ceria support-impregnated rhodium precursor in a furnace which was pre-heated at 250 ºC. The solvent used for rhodium precursor impregnation was water, as usually, and the speed at which water evaporates from the ceria-based support seemed very important for the catalyst properties, because it affected the size of the RhO_x particles on the final catalyst [7, 8]. This lead us to look for different procedures to accelerate the evaporation of the rhodium precursor solvent, and one of the options was to change water by some other more volatile solvent.

In addition, the features of the solvent used in the impregnation step not only potentially affects the distribution of the impregnated metal precursor, due to the evaporation rate, but could also had some other important roles. The optimum conditions for a successful infiltration of the support pores mainly depend on the surface polarity, the density and polarity of the solvent, and the solubility of the precursor in the solvent. For a surface with a high density of polar functional groups a polar solvent will be suitable to obtain proper wettability and suitable diffusion through the pores [9]. The density and polarity of the solvent must be also taken into account in the impregnation of honeycomb monoliths, because the solution must enter into the channels [10, 11].

As far as we know, the effect of the solvent used to impregnate praseodymium doped ceria supports with a rhodium salt on the properties of the obtained catalysts has not been reported, and the goal of the current study is to compare three solvents (water, ethanol and acetone) for such purpose.

2. Experimental

2.1. Catalyst preparation

Nine catalysts, labeled as RhO_x(solvent)/$Ce_yPr_{1-y}O_2$, were prepared. The solvent could be water, ethanol or acetone and *y* takes values of 1, 0.9 or 0.5. Cerium and praseodymium nitrate precursors ($Ce(NO_3)_3 \cdot 6H_2O$ (Aldrich, 99.99 wt.%) and ($Pr(NO_3)_3 \cdot 6H_2O$ (Aldrich, 99.9 wt.%)) were mixed in an agate mortar to obtain CeO_2, $Ce_{0.9}Pr_{0.1}O_2$ and $Ce_{0.5}Pr_{0.5}O_2$ after calcination at 600 ºC for 90

min (heating rate 10 ºC/min). Rhodium was loaded on these oxides by incipient wetness impregnation with the proper amount of $Rh(NO_3)_3 \cdot xH_2O$ (Sigma-Aldrich, ~36 wt.% as Rh) dissolved in water, ethanol or acetone in order to obtain 1 wt.% rhodium in the final catalysts. The catalysts were calcined in flash conditions, that is, the impregnated supports were introduced in a muffle furnace that was pre-heated at 250 ºC, and then the temperature was increased at 10 ºC/min up to 500 ºC (the maximum temperature was maintained for 30 min).

Additionally, three portions of pure ceria were impregnated with rhodium nitrate solutions using water, ethanol and acetone, respectively, and were placed in test tubes with a thermocouple located inside the solids. The tubes were introduced in a vertical furnace that was previously heated at 250 ºC, and the temperature was registered as a function of time.

2.2. Catalysts characterization

X-ray diffractograms were recorded in a Bruker D8-advance diffractometer, using Cu$K\alpha$ radiation (λ =1.540598 Å). Diffractograms were recorded between 10º and 80º (2θ) with steps of 0.02º and a step time of 3 sec. The average crystal size (D) was determined using the Williamson-Hall's equation.

Raman spectra were recorded in a Jobin Yvon Horiba Raman dispersive spectrometer with a variable-power He-Ne laser source (632.8 nm), 0.9 mW of power, a confocal microscope with a 10x objective of long focal length and a diffraction grating of 600 lines/mm. The spectrum of each sample was obtained

using 2 scans with an acquisition time for each individual spectrum of 200 seconds.

X-ray photoelectron spectroscopy (XPS, K-ALPHA, Thermo Scientific) was used to analyze the catalysts surface. The powder catalysts were supported on a double-sided carbon tape and were analyzed without previous pretreatment. The spectra were collected using Al-Kα radiation (1486.6 eV), monochromatized by a twin crystal monochromator, yielding a focused X-ray spot with a diameter of 400 μm, at 3 mA × 12 kV. The alpha hemispherical analyzer was operated in the constant energy mode and pass energy of 50 eV. Charge compensation was achieved with the system flood gun that provides low energy electrons and low energy argon ions from a single source. Carbon concentration on the catalysts surface amounts to 30-40 % in all cases, and the binding energy (BE) and kinetic energy (KE) scales were adjusted by setting the C1s transition at 284.6 eV.

Experiments of temperature programmed reduction with H_2 (H_2-TPR) were carried out in a Micromeritics Pulse ChemiSorb 2705 device, consisting of a tubular quartz reactor (inner diameter 5 mm) coupled to a TCD analyzer. A cold trap was placed before the TCD, consisting of a mixture of isopropyl alcohol and liquid nitrogen (temperature -89 ºC). The experiments were conducted with 20 mg of fresh catalyst at a ramp rate of 10 ºC/min from room temperature to 1050 ºC in 40 ml/min flow of 5 vol % H_2 in Ar.

Physical adsorption and desorption N_2 isotherms were obtained at -196 ºC in an automatic volumetric system (Autosorb-6, Quantachrome). Samples were outgassed at 150 ºC for 4 h under vacuum before the N_2 adsorption

measurements. The BET surface areas were determined from the N_2 adsorption isotherms.

TEM characterization was performed using a JEOL (JEM-2010) microscope, equipped with an EDS analyzer (OXFORD, model INCA Energy TEM100). A few droplets of an ultrasonically dispersed suspension of the catalyst in ethanol were placed in a copper grid with lacey carbon film and dried at ambient conditions.

2.3. N_2O decomposition tests

N_2O decomposition tests were performed in a U-shaped fix-bed quartz reactor, located in a vertical furnace at atmospheric pressure, with a 100 mL/min flow (GHSV = 42000 h^{-1}) of 1000 ppm N_2O in He, using 100 mg of catalyst. The experiments consisted of point-by-point isothermal reactions in the range of 200 – 425 ºC, increasing the temperature in intervals of 25 ºC, which were extended until the steady state was reached. The gas composition was analyzed by a HP 6890 gas chromatograph equipped with a TCD and two columns (Porapak Q, for N_2O, and Molecular Sieve 13X, for O_2 and N_2).

3. Results and discussion.

3.1. Catalysts temperature during rhodium nitrate thermal decomposition.

The effect of the solvent used for rhodium precursor impregnation on the temperature profile during the further calcination step was studied as described

148 in section 2.1. The same experiment was performed with an empty test tube.
149 The temperature profiles registered are plotted in Figure 1.

150 The temperature profile of the empty test tube shows a sharp increase
151 during approximately 5 minutes followed by a smooth increase that reaches a
152 constant value of 220 ºC (slightly lower than the set-point temperature; 250 ºC)
153 after 10 minutes. The temperature profiles of the impregnated ceria samples are
154 different. The temperature of the sample impregnated with the water solution
155 increased until 100 ºC, and reached a *plateau* at this temperature that can be
156 attributed to water evaporation. A second increase of temperature occurs
157 afterwards, reaching the same temperature than the empty tube in 15 min. The
158 samples impregnated with the ethanol or acetone solutions also exhibit solvent
159 evaporation (boiling temperature = 78 ºC and 56 ºC for ethanol and acetone,
160 respectively) but this period is much shorter than in water impregnation,
161 because a sharp increase of temperature is observed. The peak temperatures
162 reached are considerably higher than the furnace temperature. This behavior is
163 attributed to the exothermal combustion of the solvent. As it will be appealed for
164 several times throughout this article, the temperature increase occurred during
165 the thermal treatment affects the final features of the catalysts impregnated with
166 acetone or ethanol rhodium solutions.

167 *3.2.* N_2O decomposition tests.

168 N_2O decomposition tests were performed with the nine catalysts
169 prepared, and the conversion curves obtained are compiled in Figure 2.

170 The nature of the ceria-based support and the solvent used for rhodium
171 precursor impregnation affect the final activity of the catalysts. For pure ceria,

172 the type of solvent has no effect on the catalysts behavior (Figure 2.a). The
173 three RhO_x(solvent)/CeO_2 catalysts decompose N_2O from 200 ºC approximately
174 and achieve total decomposition at 375 ºC following the same decomposition
175 profile. On the contrary, the solvent used for rhodium precursor impregnation
176 strongly modifies the behavior of catalysts prepared with doped ceria supports
177 (Figures 2.b and 2.c). Regardless the molar fraction of praseodymium in doped
178 ceria, the best results were obtained with catalysts impregnated with the water
179 solution of rhodium nitrate. Both ethanol and acetone impregnations lead to a
180 significant decrease of the catalytic activity with regard to the counterpart
181 catalysts impregnated with water. The N_2O decomposition curves obtained for
182 praseodymium-containing catalysts impregnated with acetone or ethanol
183 rhodium solution were delayed by 50 - 75 ºC with regard to the curves of the
184 catalysts impregnated with water. The effect of the solvent on the
185 physicochemical properties of the catalysts, and at the end on their catalytic
186 performance, is analyzed in detail in the coming sections.

187 The temperatures required to decompose 50 % of N_2O (T_{50}) in these
188 catalytic tests have been compiled in Table 1.

189 Comparing the T_{50} values, it can be concluded that the impregnation with
190 ethanol or acetone rhodium solutions has a negative effect on catalysts
191 supported on doped ceria with regard to catalysts supported on pure ceria.
192 However, using water as the solvent, superior performance of
193 $RhO_x(H_2O)/Ce_{0.9}Pr_{0.1}O_2$ is observed with regard to catalysts with pure and 50 %
194 praseodymium doped ceria supports. The positive effect of 10 % ceria doping
195 with praseodymium is in agreement with previous publications [6]. The N_2O

196 decomposition capacity of catalysts prepared by water impregnation of rhodium
197 follows the trend:

198 $RhO_x/Ce_{0.9}Pr_{0.1}O_2 > RhO_x/CeO_2 \approx RhO_x/Ce_{0.5}Pr_{0.5}O_2$

199 According to this trend, ceria doping with 10 % praseodymium has a
200 positive effect on the catalytic activity, as already observed [6], while 50 %
201 praseodymium doping has no effect. As it will be discussed afterwards, the
202 amount of praseodymium not only affects ceria properties but also the RhO_x-
203 ceria interaction and this can explain the observed trend. For a future work, it
204 will be desirable to perform an optimization study of the praseodymium amount
205 on the $RhO_x/Ce_yPr_{1-y}O_2$ catalysts (by using water impregnation of rhodium
206 precursor), but this is out of the scope of the current study.

207 *3.3. Catalysts characterization by N_2 adsorption at -196 ºC, XRD and Raman*
208 *spectroscopy.*

209 N_2 adsorption at -196 ºC, XRD and Raman spectroscopy techniques
210 were used to analyze the physicochemical properties of the materials prepared.
211 These techniques provide (not only but mainly) information about the properties
212 of the ceria-based supports. The characterization results obtained are
213 presented in Table 2, including the BET surface area of the supports and
214 catalysts and the ceria supports crystal size and lattice parameters determined
215 by XRD.

216 The BET surface areas of all catalysts prepared with the un-doped ceria
217 support are almost equal (56-60 m^2/g), regardless the solvent used for rhodium
218 impregnation, and are also similar to that of the ceria support (61 m^2/g). In

accordance with the BET values, the ceria crystal sizes and ceria lattice parameters corresponding to these three catalysts are also similar to each other. These results allow concluding that the nature of the solvent used for rhodium impregnation do not affect the particle size/area of the pure ceria support (both parameters are related to each other in this type of oxides [12]), which is in agreement with the same catalytic activity obtained with the three praseodymium-free catalysts (see Figure 2a).

The BET surface area of the $Ce_{0.9}Pr_{0.1}O_2$ support is 50 m^2/g, which is slightly lower than that of the pure ceria. The catalysts with $Ce_{0.9}Pr_{0.1}O_2$ support impregnated with ethanol or acetone solutions present a considerably lower BET area (31-33 m^2/g) than the support, while the catalyst impregnated with the water solution of rhodium ($RhO_x(H_2O)/Ce_{0.9}Pr_{0.1}O_2$) keeps the same BET area than the support (50 m^2/g). These results must be related to the N_2O decomposition results obtained with these three $Ce_{0.9}Pr_{0.1}O_2$-supported catalysts (see Figure 2.b), that is, the highest activity was obtained with the water-impregnated catalyst (also with the highest BET surface area among catalysts of this series) and the worse catalytic results were obtained with ethanol/acetone-impregnated catalysts. As it was previously demonstrated (see Figure 1), temperature gradients are created during the calcination of catalysts impregnated with ethanol or acetone rhodium solutions while not with water. These gradients created due to the exothermic combustion of the solvents favor $Ce_{0.9}Pr_{0.1}O_2$ sintering and decrease the activity of the resulting catalysts. The BET surface area of a $Ce_{0.9}Pr_{0.1}O_2$ sample impregnated with acetone (but without rhodium) and calcined under the same conditions than the catalysts was

50 m^2/g (the same than that of fresh $Ce_{0.9}Pr_{0.1}O_2$). This evidences that rhodium catalyzes the solvents combustion.

Finally, the BET area is low and very similar for all $Ce_{0.5}Pr_{0.5}O_2$-containg catalysts (17-20 m^2/g), being also similar to that of the $Ce_{0.5}Pr_{0.5}O_2$ support. This means that rhodium impregnation and further calcination do not affects the area of this $Ce_{0.5}Pr_{0.5}O_2$ support, which is already much lower to that of CeO_2 synthesized in equal conditions (61 m^2/g). In this case, a relationship between catalytic activity and catalyst sintering during calcination is not found, since the BET areas of all $Ce_{0.5}Pr_{0.5}O_2$-containg catalysts are similar while important differences on activity were observed (see Figure 2c). As it will be demonstrated by XPS, TEM and H_2-TPR characterization afterwards, the RhO_x-$Ce_yPr_{1-y}O_2$ interaction also plays a key role on the activity of these catalysts, and the nature of the solvent used for rhodium impregnation affects such interaction.

It is important to note that, among all catalysts prepared in this study, the highest specific activity (calculated as N_2O decomposition rate per m^2 of catalyst; these plots are not shown for the sake of brevity) corresponds to $RhO_x(H_2O)/Ce_{0.5}Pr_{0.5}O_2$. This suggests that it would be desirable to focus future research to the preparation $Ce_{0.5}Pr_{0.5}O_2$ supports with higher surface area.

As a summary, the BET surface area of CeO_2 (61 m^2/g) and $Ce_{0.5}Pr_{0.5}O_2$ (18 m^2/g) does not change significantly upon rhodium impregnation and calcination, regardless the solvent used, while the area of $Ce_{0.9}Pr_{0.1}O_2$ (50 m^2/g) drops (to 31-33 m^2/g) upon rhodium impregnation with ethanol or acetone solutions and further calcination. On the contrary, there is no effect of rhodium impregnation with the water solution on the surface area of $Ce_{0.9}Pr_{0.1}O_2$.

Additional information about the features of the ceria-based supports was obtained from XRD (Figure 3) and Raman spectroscopy (Figure 4). The X-ray diffractograms only contain the main reflections of a fluorite-structured material with a face centered cubic unit cell, corresponding to the (111), (200), (220), (311), (222) and (400) planes. Evidences of segregated phases are not obvious in Figure 3. However, the presence of segregated PrO_x species is difficult to be detected by XRD, because the XRD patterns of such PrO_x species are quite similar to that of ceria [13]. Asymmetric XRD peaks could suggest the presence of segregated CeO_2-rich and PrO_x-rich phases, but this is not the case of the diffractograms in Figure 3.

The position and shape of the diffraction peaks is quite similar for all catalysts. See, for instance, the zoom of the (111) peaks inset in Figure 3. As a result, the lattice parameter of the ceria-based supports is also quite similar for all catalysts (see data in Table 2). The expansion and contraction of the crystal lattice is expected to occur due to ceria doping with large or small cations, respectively [14]. However, the sizes of the $Ce^{3+/4+}$ cations (0.114 nm/0.097 nm) are quite similar to those of the $Pr^{3+/4+}$ cations (0.113 nm/0.096 nm), and therefore, the partial substitution of cerium by praseodymium cations has a minor effect in the lattice constant of doped ceria. Slightly higher lattice constant values were obtained with some doped ceria catalysts with regard to values of catalysts with pure ceria. This must be attributed to the presence of more +3 cations, which are larger than +4 cations, mainly Pr^{3+} because Pr^{4+} is reduced more easily than Ce^{4+} [15, 16]. With regards to crystal sizes the data are consistent with the changes observed in BET surface areas, as expected [12].

292 Raman spectroscopy characterization is consistent with XRD conclusions
293 and this technique also provides evidences of praseodymium incorporation into
294 the ceria framework. As a general behavior, four Raman bands are detected on
295 the spectra included in Figure 4, but all these four bands are not seen in all
296 spectra.

297 The band at 444-463 cm^{-1} is ascribed to the Raman active F_{2g} mode of
298 fluorite ceria [17, 18]. This can be viewed as a symmetric breathing mode of the
299 oxide anions surrounding each cation. The intensity of this peak is highest for
300 catalysts with the pure ceria support (Figure 4a). A slight deformation of ceria
301 structure can be elucidated due to the introduction of praseodymium into the
302 ceria structure (in agreement with the lattice parameter calculated by XRD,
303 Table 2). The presence of Pr^{3+} cations, which are bigger than Ce^{4+}, affects the
304 oxygen breathing mode and the F_{2g} signal intensity. In addition, the
305 fluorescence produced by praseodymium also diminishes the intensity of the
306 main peak. The position of F_{2g} peak shifts towards lower Raman shifts by
307 increasing the praseodymium content, and this is also an evidence of
308 praseodymium introduction within the fluorite lattice of ceria (Figure 4).

309 The weak peak at 1170 cm^{-1}, which is not observed in all catalysts, has
310 been related to surface oxygen groups [19] and several interpretations have
311 been proposed for peaks around 200 cm^{-1} and 570 cm^{-1} [6, 14, 15, 19-22].
312 Some authors have assigned peaks at ca. 195 and 570 cm^{-1} to RhO_x species
313 [20-22] and others attributed these bands to the formation of $Ce_yPr_{1-y}O_2$ solid
314 solutions, because a physical mixture of the pure cerium and praseodymium
315 oxides did not show these features [19]. Going into more detail, these bands at

316 195 and 570 cm^{-1} have been assigned to oxygen vacancies, which affect the
317 asymmetric vibration of the oxide anions [14, 19].

318 The relative intensity of the 570 cm^{-1} band increases with regard to the
319 intensity of the main F_{2g} mode at 444-463 cm^{-1} by increasing the praseodymium
320 content (see Figure 4b and 4c), and the creation of vacant sites on ceria by
321 praseodymium doping is an evidence of solid solution formation [19].

322 *3.4. Catalysts characterization TEM, XPS and H_2-TPR.*

323 The results obtained by TEM, XPS and H_2-TPR, presented and
324 discussed in this section, provide (not only but mainly for the purposes of the
325 current study) information about the RhO_x particles and their interaction with the
326 ceria-based supports.

327 TEM images of selected catalysts are included in Figure 5. All the
328 micrographs show ceria crystals and the crystalline planes are even identified in
329 some of them. The size of the ceria-based crystals seems to be consistent with
330 the BET areas of the catalysts included in Table 2, that is, the size of the ceria-
331 based crystals observed by TEM for $RhO_x(H_2O)/CeO_2$ and
332 $RhO_x(H_2O)/Ce_{0.9}Pr_{0.1}O_2$ (60 and 50 m^2/g, respectively) are smaller than those of
333 $RhO_x(H_2O)/Ce_{0.5}Pr_{0.5}O_2$, RhO_x(acetone)/$Ce_{0.9}Pr_{0.1}O_2$ and
334 RhO_x(acetone)/$Ce_{0.5}Pr_{0.5}O_2$ (20, 33 and 18 m^2/g, respectively). The ceria
335 particles size observed by TEM also correlates with the crystal sizes obtained
336 by XRD (see Table 2).

337 Small dark spots (marked with red circles) corresponding to RhO_x
338 nanoparticles are observed in all TEM images as well. The size of these RhO_x

339 particles is smaller than 2 nm in most cases. However, a deeper TEM analysis
340 of these catalysts, and of some others of similar composition previously studied
341 [8], confirmed the presence of very small RhO_x particles (even smaller than 1
342 nm) that can be hardly observed with the magnification used to take the images
343 in Figure 5.

344 The EDS local analysis of the area of the TEM images and the global
345 analysis of the catalysts by FRX confirmed that the amount of rhodium is similar
346 in all catalysts, and therefore, the amount of RhO_x particles of ca. 2 nm
347 observed in the TEM images of Figure 5 can be related with RhO_x dispersion. If
348 RhO_x is highly dispersed only few RhO_x particles are observed in the TEM
349 images, because most RhO_x particles are below the detection limit of the
350 technique. On the contrary, a lot of RhO_x spots are observed in a TEM image
351 when RhO_x is less dispersed.

352 Comparing the three TEM images (Figure 5) of catalysts prepared by
353 water impregnation of rhodium nitrate, it is observed that there are much more
354 RhO_x particles on the catalyst with $Ce_{0.5}Pr_{0.5}O_2$ support than on those with
355 $Ce_{0.9}Pr_{0.1}O_2$ or CeO_2, and this is an evidence of the worst RhO_x dispersion over
356 $Ce_{0.5}Pr_{0.5}O_2$. This lower RhO_x dispersion on $RhO_x(H_2O)/Ce_{0.5}Pr_{0.5}O_2$ is
357 coincident with the lowest BET area of this catalyst (see data in Table 2). On
358 the other hand, more RhO_x particles are observed on
359 RhO_x(acetone)/$Ce_{0.9}Pr_{0.1}O_2$ than on $RhO_x(H_2O)/Ce_{0.9}Pr_{0.1}O_2$, which could be
360 related with the BET area values (60 and 33 m^2/g, respectively).

361 The conclusion of this TEM characterization is that both the nature of the
362 ceria-based support and of the solvent used for rhodium impregnation affect

363 RhO_x dispersion. As a general trend, RhO_x dispersion on CeO_2 and $Ce_{0.9}Pr_{0.1}O_2$
364 is better than on $Ce_{0.5}Pr_{0.5}O_2$, and RhO_x dispersion is better for water-
365 impregnated catalysts than for ethanol or acetone-impregnated catalysts. Some
366 of these conclusions are supported by the XPS characterization.

367 Figure 6 shows the Rh 3d photoelectron spectra of all catalysts. Two
368 peaks are observed in all spectra, corresponding to the $3d_{5/2}$ and $3d_{3/2}$
369 transitions (around 309 and 313 eV, respectively). Both peaks provide similar
370 information about the oxidation state of rhodium. The position of the Rh $3d_{5/2}$
371 peaks is 309.0–310.0 eV for all catalysts, which corresponds to Rh^{3+} cations. As
372 reported in the literature, the Rh $3d_{5/2}$ peak appears at 307.0–307.5 eV for Rh^0,
373 at about 308 eV for Rh^+, and from 308.3 to 310.5 eV for Rh^{3+} [23-25].

374 There are subtle differences in the position of the Rh 3d peaks in Figure
375 6 that deserve a detailed analysis. In RhO_x-ceria catalysts, there is a negative
376 charge density transfer from the noble metal to the ceria support, and the extent
377 of such transfer affects the position of the Rh 3d peaks.

378 The position of the $3d_{5/2}$ peak is 309.5 eV for all RhO_x/CeO_2 catalysts
379 (Figure 6.a), regardless the solvent used for rhodium impregnation, while it is
380 shifted to slightly higher values for $RhO_x/Ce_{0.9}Pr_{0.1}O_2$ catalysts (Figures 6.b) and
381 to lower values for $RhO_x/Ce_{0.5}Pr_{0.5}O_2$ (Figures 6.c). This means that the RhO_x-
382 support interaction strongly depends on the support nature, and ceria doping
383 with 10 % praseodymium favors the RhO_x-support interaction while 50 %
384 praseodymium doping hinders the interaction. This is consistent with the lowest
385 BET area of this support (see Table 2). The reason of the positive effect of 10%
386 praseodymium doping while negative of 50% praseodymium doping seems to

be that cerium is the main responsible of the charge density transfer from Rh(III) to the support while praseodymium modifies the cerium behavior. Both cerium and praseodymium can adopt the 3+ and 4+ oxidation states, but praseodymium is more prone to form the +3 cation (see Table 3 and discussion below). It is expected that the charge density transfer from Rh^{3+} to the support occurs with (Ce and Pr) 4+ cations rather than with +3 cations, and therefore, cerium should interact more efficiently with rhodium than praseodymium. Few praseodymium doping (10%) has a positive effect because promotes the interaction of Ce^{4+} cations with rhodium, that is, the presence of Pr favors the formation of vacant sites on the support and improves oxygen mobility, and this favors the charge density transfer (oxide anions at the end) from rhodium to ceria. 50% praseodymium doping also has this positive effect, but due to the high diluting effect there is less cerium available to interact with rhodium.

The cerium and praseodymium oxidation states have been estimated by XPS, and the values obtained are compiled in Table 3 together with the Ce/Pr surface ratios. The Ce^{3+} percentage (with regard to total surface cerium) was estimated following the method proposed elsewhere [6] and the Pr^{3+} percentage (with regard to total surface praseodymium) by using the semi-quantitative method proposed by Borchert et al. [26]. The percentage of Ce^{3+} is similar for all catalysts prepared with the pure ceria support (34-37 %) and these percentages slightly decrease upon praseodymium doping, evidencing the insertion of the dopant into the ceria lattice. The Pr^{3+} percentages are much higher than those of Ce^{3+} due to the easier reducibility of Pr^{4+} with regard to Ce^{4+}. Moreover, the presence of Pr^{3+} cations partially decreases the reduction of Ce^{4+}.

412 Regarding the Ce/Pr ratios, they are well below the expected nominal
413 ratios deduced from the stoichiometric formula of the mixed oxides (9 for
414 $Ce_{0.9}Pr_{0.1}O_2$ and 1 for $Ce_{0.5}Pr_{0.5}O_2$). Rodríguez-Luque et al. [27] reported the
415 rhodium nanocrystallites decoration by patches of support in
416 Rhodium/$Ce_yPr_{1-y}O_2$ catalysts. It was argued that, during rhodium impregnation,
417 the acid character of the rhodium solution promotes Pr^{3+} leaching, and after
418 catalyst drying and calcination, such species are accumulated on the particles
419 surface. This would explain the preferential accumulation of praseodymium on
420 the surface of our catalysts.

421 As a summary, the XPS analysis suggests that praseodymium is partially
422 inserted into the ceria lattice for catalysts with doped ceria supports, but with an
423 enrichment of praseodymium on the particles surface. Such praseodymium
424 doping affects the RhO_x-support interaction, being improved for 10 %
425 praseodymium doping but hindered for 50 % doping.

426 The RhO_x-support interaction is known to affect the RhO_x/ceria catalysts
427 reducibility, which is closely related to the catalytic activity for N_2O
428 decomposition. In order to study such reducibility, H_2-TPR experiments were
429 performed and the profiles obtained are compiled in Figure 7.

430 Three peaks are shown in most H_2-reduction profiles, as expected [5,
431 28]. The lowest-temperature peak can be attributed to the reduction of RhO_x,
432 and, in some cases, also to the rhodium-catalyzed ceria-based support surface
433 reduction. The intermediate-temperature peak is attributed by some authors to
434 surface ceria reduction as well, but not catalyzed by the noble metal, whereas
435 other authors relate this peak to surface and/or bulk carbonates decomposition

436 [29] and/or to surface hydroxyls, peroxides or superoxides reduction. Finally,
437 the peak at highest temperature is attributed to bulk ceria-support reduction.

438 Special attention must be paid to the lowest temperature reduction peak
439 [6], mainly taking into account the symmetry of the peak. The catalysts with high
440 activity for N_2O decomposition, which are those prepared with the pure ceria
441 support and those impregnated with a water solution of rhodium, regardless the
442 support (see Figure 2), present a single low-temperature H_2 reduction peak. On
443 the contrary, two overlapped peaks are evident in catalysts with lower activity,
444 which are those impregnated with acetone or ethanol solutions in doped ceria
445 supports [6, 7].

446 The presence of double-peaks or pronounced shoulders in the lowest
447 temperature H_2 reduction peaks occur because Rh^{3+}, Pr^{4+} and Ce^{4+} are reduced
448 sequentially, while symmetric peaks are obtained if such reductions occur
449 simultaneously [7]. Therefore, the shape of this peak is related with the RhO_x-
450 support interaction and with the formation of doped ceria solid solutions. The
451 catalysts with good RhO_x-support interaction present high catalytic activity [5]. It
452 has been reported that the most active sites for N_2O decomposition are located
453 at the RhO_x-ceria interface [30]. Also, a very effective N_2O decomposition has
454 been demonstrated to occur on RhO_x/ceria catalysts, and a synergy between
455 rhodium and ceria catalytic sites was proposed. This effective mechanism
456 needs a good RhO_x-ceria interaction [17].

457 The highest temperature peak attributed to bulk reduction disappeared
458 by increasing the amount of praseodymium. This is due to the improved

459 reducibility with regard to pure ceria, which is related to the enhanced oxygen
460 mobility into the lattice [6].

461 In conclusion, the activity for N_2O decomposition of the catalysts studied
462 is related with the RhO_x-support interaction. Both the nature of the ceria support
463 and the solvent used for rhodium precursor impregnation affect such interaction.
464 Ceria doping with 10 % praseodymium has a positive effect on such interaction
465 (see XPS results; Figure 6) and on the catalytic activity (see Figure 2 and Table
466 1), but the benefit on the catalytic activity is only obtained using a water solution
467 for impregnation. On the contrary, when $Ce_{0.9}Pr_{0.1}O_2$ is impregnated with
468 ethanol or acetone solutions of rhodium, the temperature gradients created
469 during calcination (Figure 1) promote the support (see BET areas in Table 2)
470 and RhO_x sintering (see RhO_x sizes on TEM images; Figure 5), hindering the
471 RhO_x-$Ce_{0.9}Pr_{0.1}O_2$ interaction. The interaction between RhO_x and $Ce_{0.5}Pr_{0.5}O_2$ is
472 not as good as that with $Ce_{0.9}Pr_{0.1}O_2$ (see the XPS binding energies of Rh^{3+}
473 (Figure 6)), but it seems to be enough to keep a high catalytic activity if the
474 impregnation is carried out with a water solution. In fact, the H_2-TPR peak at low
475 temperature (Figure 7.c) demonstrates a considerable RhO_x-support interaction.
476 However, acetone or ethanol impregnation also leads to an important decrease
477 in activity, and this must be attributed to a worst RhO_x-support interaction.
478 Finally, pure CeO_2 is more stable towards sintering than doped ceria under the
479 calcination conditions of this study (contrary to the phenomenon observed at
480 high-temperature calcination).Pure ceria does not sinter regardless the solvent
481 used for rhodium impregnation, and for this reason all the RhO_x/CeO_2 catalysts
482 kept the same activity.

This study suggests that the best catalyst is obtained by impregnating $Ce_{0.9}Pr_{0.1}O_2$ with a water solution of rhodium precursor. However, if acetone or ethanol must be used for any reason (to improve wettability of a honeycomb monolith channels, for instance) the pure ceria support is more suitable.

4. Conclusions.

The effect of the solvent (water, ethanol or acetone) used to impregnate $Ce_yPr_{1-y}O_2$ (y = 1, 0.9 or 0.5) supports with rhodium nitrate, in order to prepare N_2O decomposition catalysts, have been studied and the following main conclusions can be summarized:

- Both the nature of the ceria support and the solvent used for rhodium precursor impregnation affect the RhO_x-support interaction and the activity for N_2O decomposition.

- The use of ethanol or acetone as solvent has a very negative effect on $Ce_{0.9}Pr_{0.1}O_2$ and $Ce_{0.5}Pr_{0.5}O_2$-containing catalysts, due to the sintering of both the support and RhO_x particles. This affects negatively the RhO_x-support interaction which directly hinders the catalytic activity for N_2O decomposition. This negative effect is due to the rhodium-catalyzed solvent combustion.

- Ceria doping with 10 % praseodymium has a positive effect on the RhO_x-support interaction (and on the catalytic activity), which is observed as a negative charge density transfer from the noble metal to the ceria support (only obtained using water for impregnation).

- The interaction between RhO_x and $Ce_{0.5}Pr_{0.5}O_2$ is not as good as that with $Ce_{0.9}Pr_{0.1}O_2$, but it is enough to keep a high catalytic activity if rhodium is impregnated with a water solution. However, acetone or ethanol impregnation leads to an important decrease in activity, and this must be attributed to the worst interaction of RhO_x with the support, as deduced from the shape of the lowest temperature H_2-TPR peaks.

Acknowledgments

The authors thank the financial support of Generalitat Valenciana (Project Prometeo 2009/047), the Spanish Ministry of Economy and Competitiveness (Project CTQ2012-30703), and the UE FEDER funding.

References.

[1] A. Trovarelli, Catal. Rev. Sci. Eng. 38 (1996) 439.

[2] A. Trovarelli, C. De Leitenburg, M. Boaro, G. Dolcetti, Catal. Today 50 (1999) 353.

[3] M. Shelef, G. W. Graham, R. W. McCabe, in: A. Trovarelli (ed), Catalysis by ceria and related materials Catalytic Science Series. Vol. 2, Imperial College Press,2002, pp 343-376.

[4] J. Kašpar, P. Fornasiero, N. Hickey, Catalysis Today 77 (2003) 419.

[5] S. Imamura, J. Tadani, Y. Saito, Y. Okamoto, H. Jindai, C. Kaito, Appl. Catal. A 201 (2000) 121.

[6] A. Bueno-López, I. Such-Basáñez, C. Salinas-Martínez de Lecea, J. Catal. 244 (2006) 102.

[7] V. Rico-Pérez, S. Parres-Esclapez, M.J. Illán-Gómez, C. Salinas-Martínez de Lecea, A. Bueno-López, Appl. Catal. B 107 (2011) 18.

[8] V. Rico-Pérez, M.A. Velasco-Beltrán, Q. He, Q. Wang, C. Salinas-Martínez de Lecea, A. Bueno-López, Catal. Commun. 33 (2013) 47.

[9] J. Roggenbuck, T. Waitz, M. Tiemann, Micropor. Mesopor. Mat. 113 (2008) 575.

[10] T.A. Nijhuis, A.E.W. Beers, T. Vergunst, I. Hoek, F. Kapteijn, J.A. Moulijn, Cat. Rev. Sci. Eng. 43 (2001) 345.

[11] L. C. Almeida, F. J. Echave, O. Sanz, M. A. Centeno, J. A. Odriozola, M. Montes. Stud. Surf. Sci. Catal. 175 (2010) 25.

[12] C. Bueno-Ferrer, S. Parres-Esclapez, D. Lozano-Castelló, A. Bueno-López. J. Rare Earths 28 (2010) 647.

[13] H. He, H.X. Dai, C.T. Au, Catal. Today 90 (2004) 245.

[14] J.R. McBride, K.C. Hass, B.D. Poindexter, W.H. Weber, J. Appl. Phys. 76 (1994) 2435.

[15] S. Bernal, G. Blanco, M.A. Cauqui, A. Martiın, J.M. Pintado, A. Galtayries, R. Sporken, Surf. Int. Anal. 30 (2000) 85.

[16] K. Aboussaid, S. Bernal, G. Blanco, J. J. Calvino, G. A. Cifredo, M. Lopez-Haro, J. M. Pintado, M. S. el Begrani, O. Stephan, S. Trasobares, Surf. Int. Anal. 40 (2008) 242.

[17] S. Parres-Esclapez, I. Such-Basáñez, M.J. Illán-Gómez, C. Salinas-Martínez de Lecea, A. Bueno-López, J. Catal. 276 (2010) 390.

[18] M. Yashima, H. Arashi, M. Kakihana, M. Yoshimura, J. Americ. Ceram. Soc. 77 (1994) 1067.

[19] M-F. Luo, Z-L. Yan, L-Y. Jin, J. Molec. Catal. A: Chem. 260 (2006) 157.

[20] S. Music, A. Saric, S. Popovic, M. Ivanda, J. Molec. Struct. 924–926 (2009) 221.

[21] M. Kurnatowska, L. Kepinski, Mat. Res. Bull. 48 (2013) 852.

[22] V.V. Pushkarev, V.I. Kovalchuk, J.L. d'Itri, J. Phys. Chem. B 108 (2004) 5341.

[23] http://www.lasurface.com. Access May 2013

[24] X.D. Wu, L.H. Xu, D. Weng, Appl. Surf. Sci. 221 (2004) 375.

[25] J. Soria, A. Martínez-Arias, J.L.G. Fierro, J.C. Conesa, Vacuum 46 (1995) 1201.

[26] H. Borchert, Y.V. Frolova, V.V. Kaichev, I.P. Prosvirin, G.M. Alikina, A.I. Lukashevich, V.I. Zaikovskii, E.M. Moroz, S.N. Trukhan, V.P. Ivanov, E.A. Paukshtis, V.I. Bukhtiyarov, V.A. Sadykov, J. Phys. Chem. B 109 (2005) 5728.

[27] M.P. Rodríguez-Luque, J.C. Hernandez, M.P. Yeste, S. Bernal, M.A. Cauqui, J.M. Pintado, J.A. Perez-Omil, O. Stephan, J.J. Calvino, S. Trasobares. J. Phys. Chem. C 112 (2008) 5900.

[28] P. Fornasiero, P. Di Monte, G.R. Rao, J. Kaspar, S. Meriani, A. Trovarelli, M. Graziani, J. Catal. 151 (1995) 168.

[29] F.M.Z. Zotin, L. Tournayan, J. Varloud, V. Perrichon, R. Frety, Appl. Catal. A 98 (1993) 99.

[30] J. Cunningham, J.N. Hickey, R. Cataluna, J.C. Conesa, J. Soria, A. Martínez-Arias. Stud. Surf. Sci. Catal. 101 (1996) 681.

Table 1. Temperature required to decompose 50% of N_2O (T_{50}) in the catalytic tests.

Catalyst	T_{50} (ºC)
$RhO_x(H_2O)/CeO_2$	252
RhO_x(ethanol)/CeO_2	252
RhO_x(acetone)/CeO_2	252
$RhO_x(H_2O)/Ce_{0.9}Pr_{0.1}O_2$	242
RhO_x(ethanol)/$Ce_{0.9}Pr_{0.1}O_2$	287
RhO_x(acetone)/$Ce_{0.9}Pr_{0.1}O_2$	301
$RhO_x(H_2O)/Ce_{0.5}Pr_{0.5}O_2$	252
RhO_x(ethanol)/$Ce_{0.5}Pr_{0.5}O_2$	326
RhO_x(acetone)/$Ce_{0.}5Pr_{0.5}O_2$	319

Table 2. Results of the N_2 adsorption and XRD characterization.

Sample	BET surface area (m^2/g)	Crystal size (nm)	Lattice parameter (nm)
CeO_2	61	-	-
$RhO_x(H_2O)/CeO_2$	60	14	0.5413
RhO_x(ethanol)/CeO_2	60	14	0.5412
RhO_x(acetone)/CeO_2	56	15	0.5412
$Ce_{0.9}Pr_{0.1}O_2$	50	-	-
$RhO_x(H_2O)/Ce_{0.9}Pr_{0.1}O_2$	50	18	0.5417
RhO_x(ethanol)/$Ce_{0.9}Pr_{0.1}O_2$	31	21	0.5416
RhO_x(acetone)/$Ce_{0.9}Pr_{0.1}O_2$	33	21	0.5415
$Ce_{0.5}Pr_{0.5}O_2$	18	-	-
$RhO_x(H_2O)/Ce_{0.5}Pr_{0.5}O_2$	20	24	0.5412
RhO_x(ethanol)/$Ce_{0.5}Pr_{0.5}O_2$	17	21	0.5420
RhO_x(acetone)/$Ce_{0.5}Pr_{0.5}O_2$	18	21	0.5420

Table 3. Ce^{3+} and Pr^{3+} percentages (with regard to total Ce and Pr surface contents, respectively) and Ce/Pr atomic ratio determined by XPS.

	Ce^{3+} (%)	**Pr^{3+} (%)**	**Ce/Pr**
$RhO_x(H_2O)/CeO_2$	37	-	-
RhO_x(ethanol)/CeO_2	35	-	-
RhO_x(acetone)/CeO_2	34	-	-
$RhO_x(H_2O)/Ce_{0.9}Pr_{0.1}O_2$	28	58	4.0
RhO_x(ethanol)/$Ce_{0.9}Pr_{0.1}O_2$	30	72	3.4
RhO_x(acetone)/$Ce_{0.9}Pr_{0.1}O_2$	28	66	3.7
$RhO_x(H_2O)/Ce_{0.5}Pr_{0.5}O_2$	31	51	0.6
RhO_x(ethanol)/$Ce_{0.5}Pr_{0.5}O_2$	30	66	0.7
RhO_x(acetone)/$Ce_{0.5}Pr_{0.5}O_2$	30	50	0.7

Figure captions

Figure 1. Temperature profiles during the thermal treatment of ceria-impregnated rhodium precursor (using water, ethanol or acetone as solvent) in test tubes placed in a vertical furnace pre-heated at 250 ºC.

Figure 2. N_2O decomposition as a function of temperature for catalysts supported on: (a) CeO_2, (b) $Ce_{0.9}Pr_{0.1}O_2$ and (c) $Ce_{0.5}Pr_{0.5}O_2$.

Figure 3. X-ray diffractograms of catalysts supported on (a) CeO_2, (b) $Ce_{0.9}Pr_{0.1}O_2$ and (c) $Ce_{0.5}Pr_{0.5}O_2$. Diffractograms 1, 4, 7 correspond to samples impregnated with ethanol solution; 2, 5, 8 to samples impregnated with acetone solution and 3, 6, 9 to samples impregnate with water solution.

Figure 4. Raman spectra of catalysts with RhOx supported on (a) CeO_2, (b) $Ce_{0.9}Pr_{0.1}O_2$ and (c) $Ce_{0.5}Pr_{0.5}O_2$ (c).

Figure 5. TEM images of catalysts (a) $RhO_x(H_2O)/CeO_2$, (b) $RhO_x(H_2O)/Ce_{0.9}Pr_{0.1}O_2$, (c) $RhO_x(H_2O)/Ce_{0.5}Pr_{0.5}O_2$, (d) RhO_x(acetone)/$Ce_{0.9}Pr_{0.1}O_2$, (e) RhO_x(acetone)/$Ce_{0.5}Pr_{0.5}O_2$. RhOx particles have been circled.

Figure 6. Rh 3d XPS spectra of catalysts with RhOx supported on (a) CeO_2, (b) $Ce_{0.9}Pr_{0.1}O_2$ and (c) $Ce_{0.5}Pr_{0.5}O_2$.

Figure 7. H_2-TPR profiles of catalysts with RhOx supported on (a) CeO_2, (b) $Ce_{0.9}Pr_{0.1}O_2$ and (c) $Ce_{0.5}Pr_{0.5}O_2$.

Figure 1.

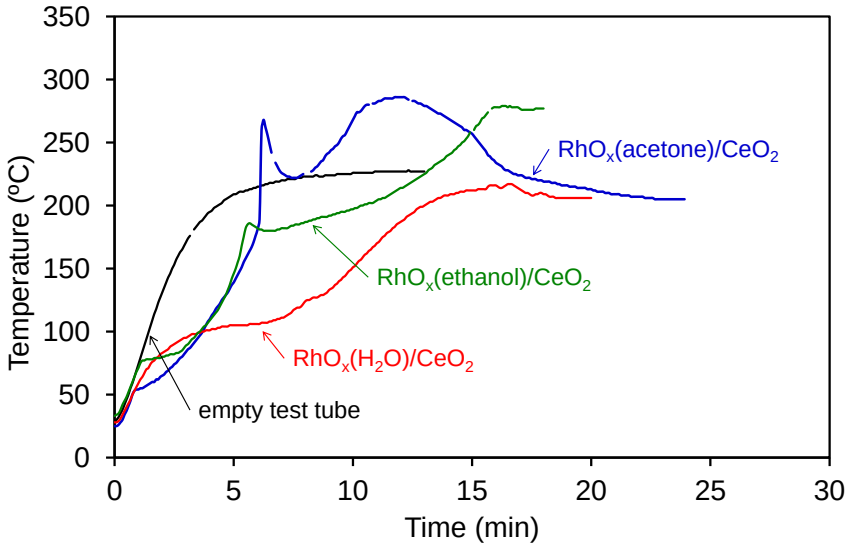
350
300
250
200
150
100
50
0
Temperature (ºC)
0
5
10
15
20
25
30
Time (min)
RhO$_x$(acetone)/CeO$_2$
RhO$_x$(ethanol)/CeO$_2$
RhO$_x$(H$_2$O)/CeO$_2$
empty test tube

Figure 2.

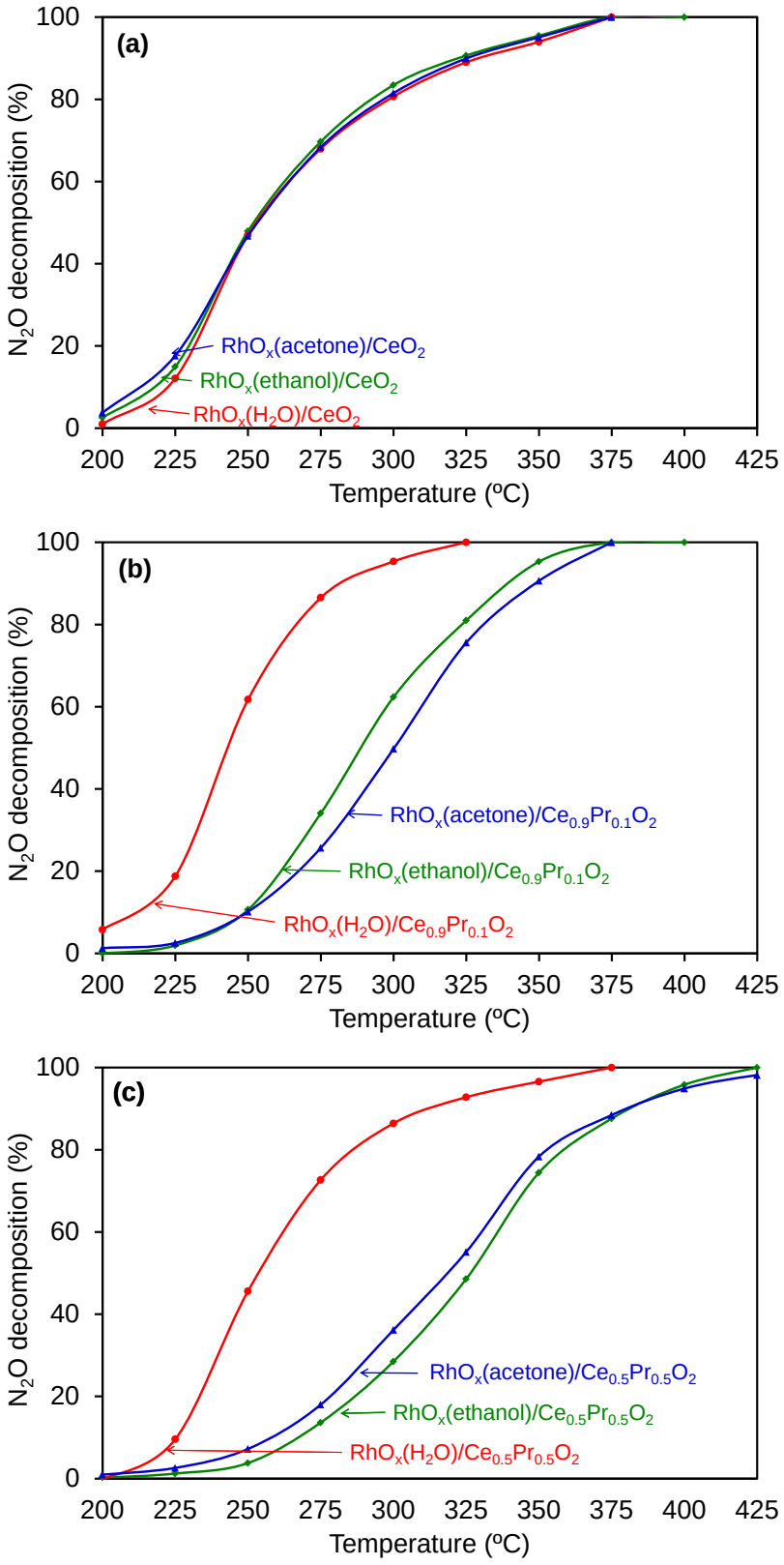
(a)
N2O decomposition (%)
Temperature (ºC)
RhOx(acetone)/CeO2
RhOx(ethanol)/CeO2
RhOx(H2O)/CeO2
(b)
N2O decomposition (%)
Temperature (ºC)
RhOx(acetone)/Ce0.9Pr0.1O2
RhOx(ethanol)/Ce0.9Pr0.1O2
RhOx(H2O)/Ce0.9Pr0.1O2
(c)
N2O decomposition (%)
Temperature (ºC)
RhOx(acetone)/Ce0.5Pr0.5O2
RhOx(ethanol)/Ce0.5Pr0.5O2
RhOx(H2O)/Ce0.5Pr0.5O2

Figure 3.

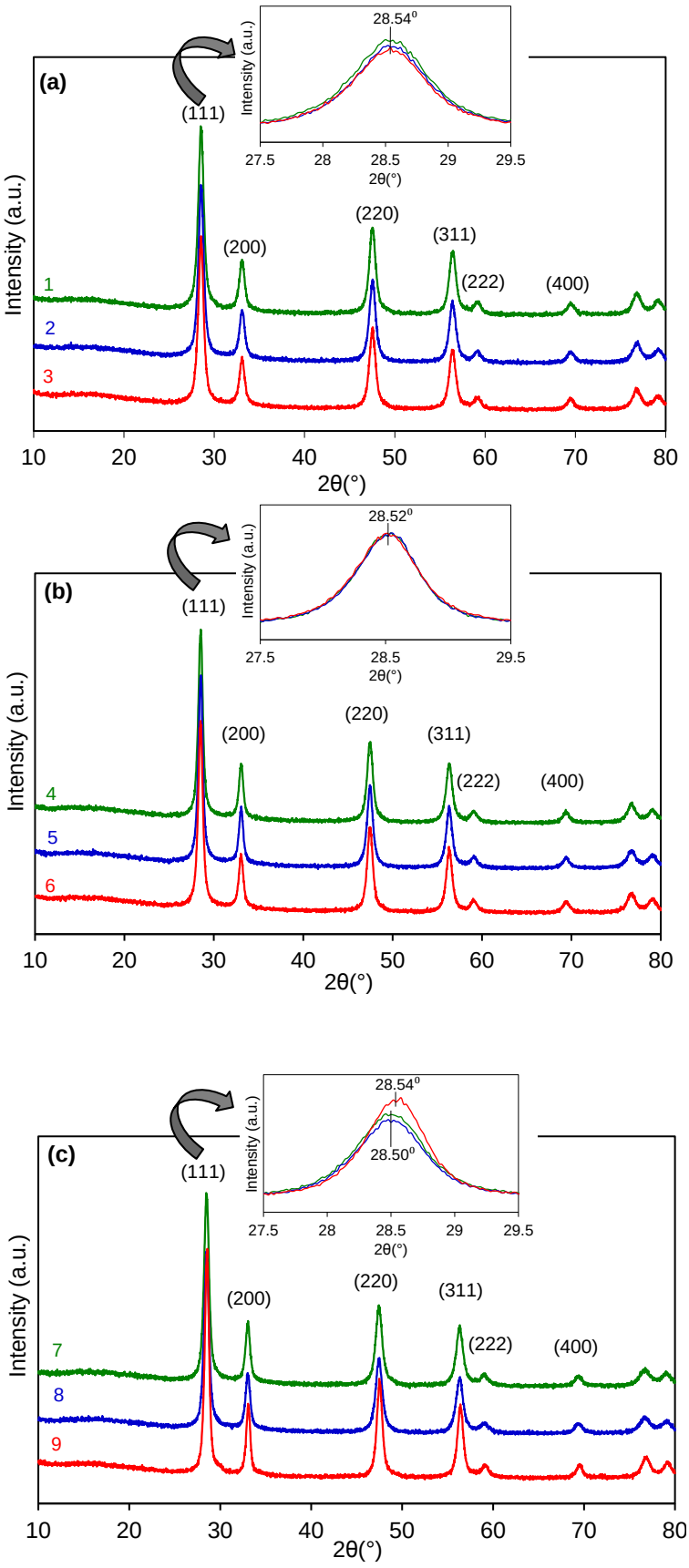
(a)
(111)
(200)
(220)
(311)
(222)
(400)
1
2
3
Intensity (a.u.)
2θ(°)
28.54⁰
(b)
28.52⁰
4
5
6
(c)
28.54⁰
28.50⁰
7
8
9

Figure 4.

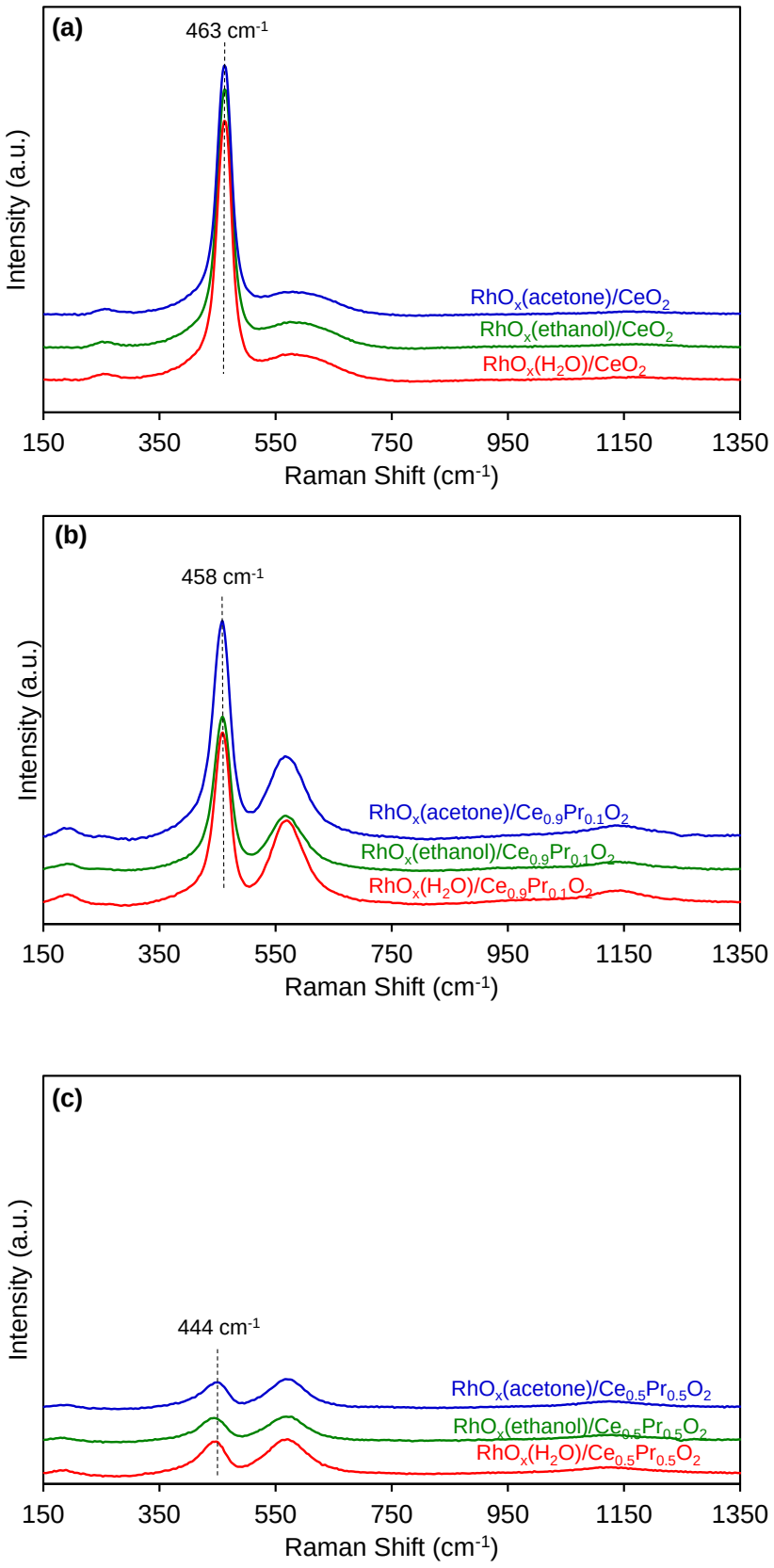
(a)
463 cm-1
Intensity (a.u.)
RhOx(acetone)/CeO2
RhOx(ethanol)/CeO2
RhOx(H2O)/CeO2
150
350
550
750
950
1150
1350
Raman Shift (cm-1)
(b)
458 cm-1
Intensity (a.u.)
RhOx(acetone)/Ce0.9Pr0.1O2
RhOx(ethanol)/Ce0.9Pr0.1O2
RhOx(H2O)/Ce0.9Pr0.1O2
150
350
550
750
950
1150
1350
Raman Shift (cm-1)
(c)
444 cm-1
Intensity (a.u.)
RhOx(acetone)/Ce0.5Pr0.5O2
RhOx(ethanol)/Ce0.5Pr0.5O2
RhOx(H2O)/Ce0.5Pr0.5O2
150
350
550
750
950
1150
1350
Raman Shift (cm-1)

Figure 5.

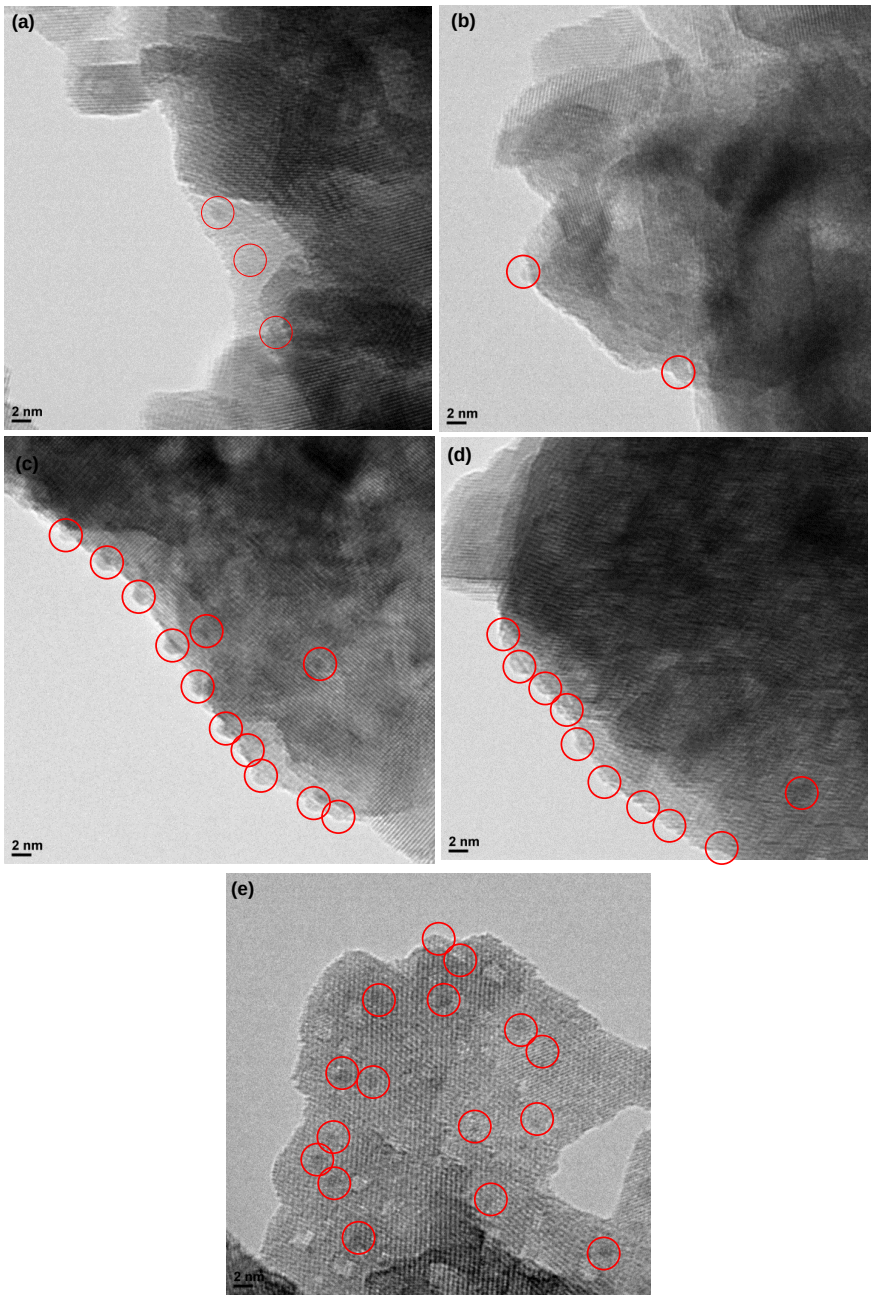

Figure 6.

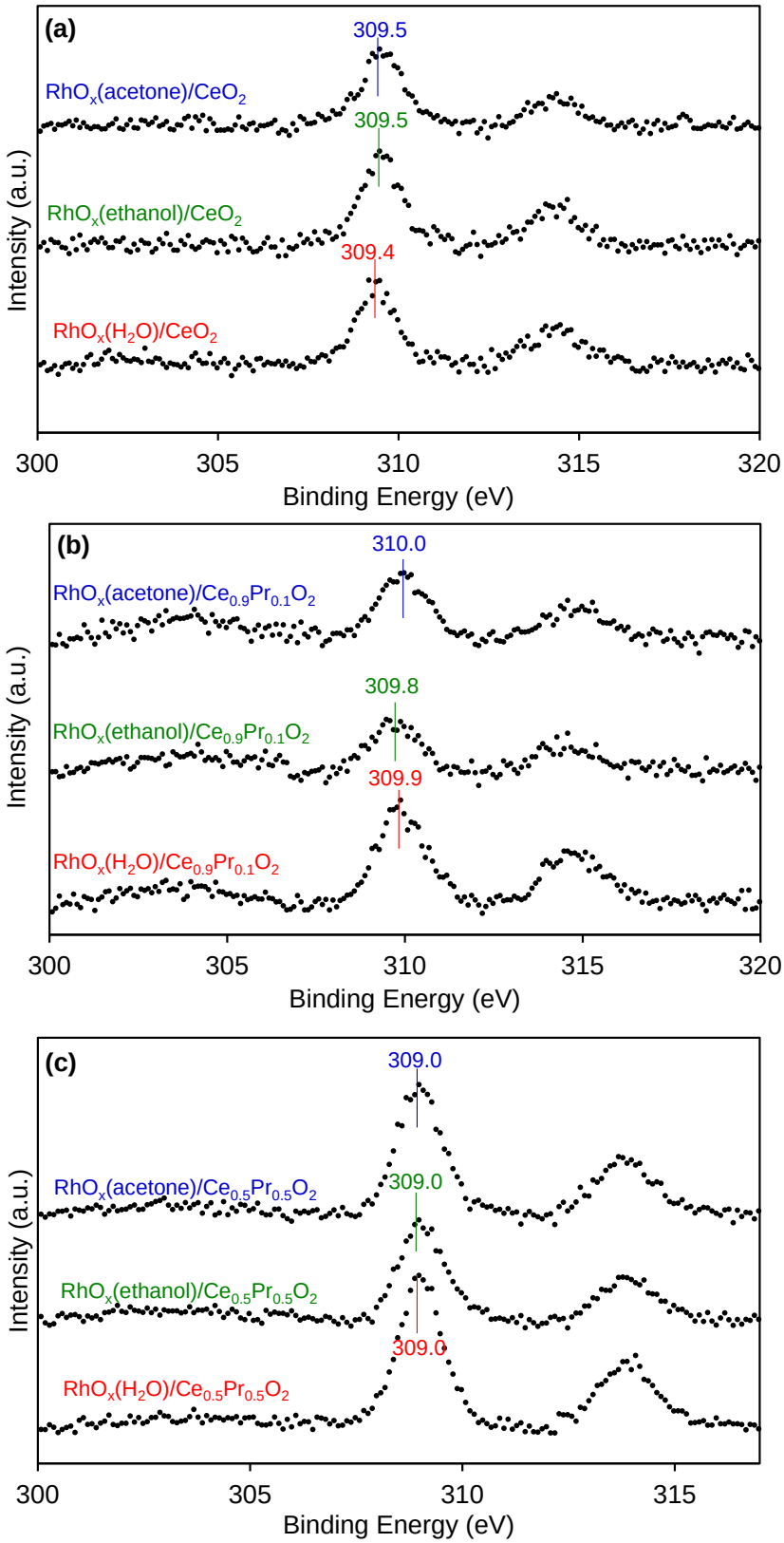
(a)
309.5
RhOx(acetone)/CeO2
309.5
RhOx(ethanol)/CeO2
309.4
RhOx(H2O)/CeO2
Intensity (a.u.)
300
305
310
315
320
Binding Energy (eV)
(b)
310.0
RhOx(acetone)/Ce0.9Pr0.1O2
309.8
RhOx(ethanol)/Ce0.9Pr0.1O2
309.9
RhOx(H2O)/Ce0.9Pr0.1O2
Intensity (a.u.)
300
305
310
315
320
Binding Energy (eV)
(c)
309.0
RhOx(acetone)/Ce0.5Pr0.5O2
309.0
RhOx(ethanol)/Ce0.5Pr0.5O2
309.0
RhOx(H2O)/Ce0.5Pr0.5O2
Intensity (a.u.)
300
305
310
315
Binding Energy (eV)

Figure 7.

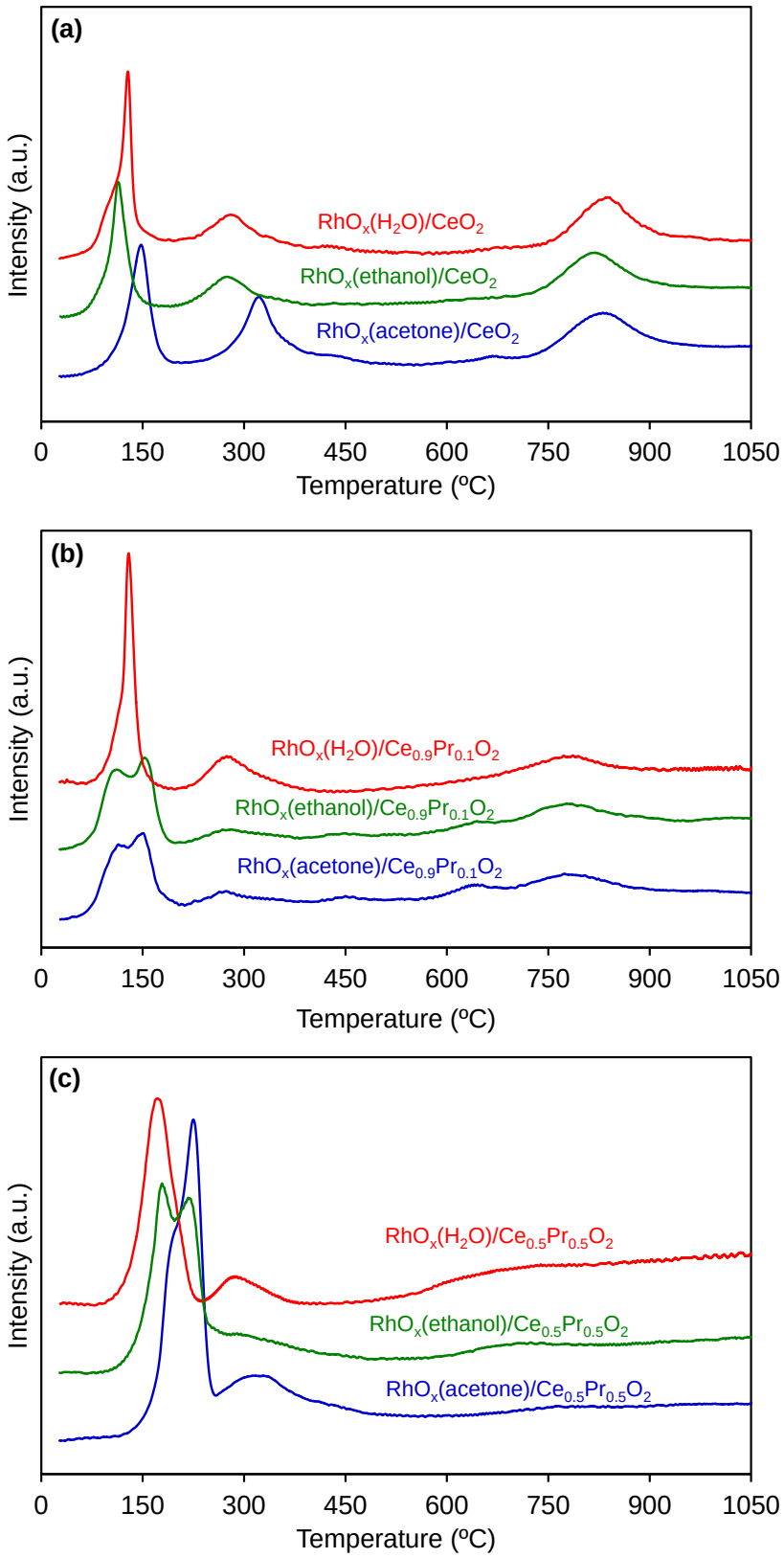
(a)
Intensity (a.u.)
RhOx(H2O)/CeO2
RhOx(ethanol)/CeO2
RhOx(acetone)/CeO2
0
150
300
450
600
750
900
1050
Temperature (ºC)
(b)
Intensity (a.u.)
RhOx(H2O)/Ce0.9Pr0.1O2
RhOx(ethanol)/Ce0.9Pr0.1O2
RhOx(acetone)/Ce0.9Pr0.1O2
0
150
300
450
600
750
900
1050
Temperature (ºC)
(c)
Intensity (a.u.)
RhOx(H2O)/Ce0.5Pr0.5O2
RhOx(ethanol)/Ce0.5Pr0.5O2
RhOx(acetone)/Ce0.5Pr0.5O2
0
150
300
450
600
750
900
1050
Temperature (ºC)